Proceedings of DSCC2008
2008 ASME Dynamic Systems and Control Conference
October 20-22, 2008, Ann Arbor, Michigan, USA

DSCC2008-2287

EXPLANATION FOR LOW-SPEED STABILITY INCREASES IN MACHINING: APPLICATION OF A CONTINUOUS DELAY MODEL

Firas A. Khasawneh*
Brian P. Mann
Department of Mechanical Engineering and Materials Science
Duke University
Durham, North Carolina 27708
Email: firas.khasawneh@duke.edu
brian.mann@duke.edu

Tamás Insperger
Gabor Stépán
Department of Applied Mechanics
Budapest University of Technology and Economics, H-1521
Budapest, Hungary
Email: inspi@mm.bme.hu
stepan@mm.bme.hu

ABSTRACT

This paper investigates the analysis of delay integro-differential equations to explain the increased stability behavior commonly observed at low cutting speeds in machining processes. In the past, this improved stability has been attributed to the energy dissipation from the interference between the workpiece and the tool relief face. In this study, an alternative physical explanation is described. In contrast to the conventional approach, which uses a point force acting at the tool tip, the cutting forces are distributed over the tool-chip interface. This approximation results in a second order delayed integro-differential equation for the system that involves a short and a discrete delay. A method for determining the stability of the system for an exponential shape function is described, and temporal finite element analysis is used to chart the stability regions. Comparisons are then made between the stability charts that use the conventional point force and those that use the distributed force model for continuous and interrupted turning.

INTRODUCTION

A normal phenomenon associated with cutting operations is relative vibrations between the tool and the workpiece. When these vibrations become unstable, they are commonly referred to as chatter which may result in defective machined parts and increased tool wear. Chatter can also damage the workpiece, the fixture and/or the machine spindle. Mapping the areas of stability as a function of the machining parameters, namely the depth of cut and the spindle speed, not only helps avoid these detrimental effects of chatter but also increases the efficiency of the cutting process. Predictive models that can generate stability regions for a wide combination of speeds and cutting depths eliminate the costly and time-consuming trial and error alternative.

In order to generate the stability charts for a cutting operation, it is necessary to model the system dynamics through suitable equations of motion, descriptive force models and apply proper solution techniques. Models describing cutting tool vibrations began to appear in literature about half a century ago [1–4]. Several models have been proposed to characterize the cutting forces as a function of the cutting parameters, such as the depth of cut and the instantaneous chip thickness whose product forms the instantaneous chip area. These models treated cutting forces as a point force acting at the tool tip. This conventional approximation of the cutting forces has been verified experimentally in the middle range of cutting speeds. However, actual observations of the cutting process at low speeds show improved stability when compared to those obtained from theoretical predictions, (e.g. see Fig. 1).

There are many machining operations that can be performed only at low speeds. For instance, harder to machine materials, like stainless steel and titanium, are used extensively in medical tool manufacturing and in the spacecraft industry. Titanium, for example, has very high strength to weight ratio and excellent corrosion resistance, which makes it ideal for aerospace applications [5]. Titanium also has great bio-compatibility so it is widely used in medical implants [6]. However, titanium is difficult to machine owing to its inherent properties of high strength combined with poor thermal conductivity. This requires titanium to be machined only at low speeds.

*Corresponding author

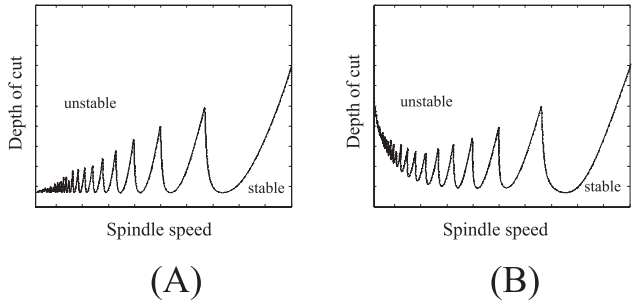

Figure 1. QUALITATIVE STABILITY CHARTS SHOWN TO ILLUSTRATE THE PHENOMENOLOGICAL INCREASE IN STABILITY AT RELATIVELY LOW CUTTING SPEEDS. GRAPH (A) SHOWS THE STABILITY BOUNDARIES FOR A TYPICAL POINT FORCE MODEL AND GRAPH (B) PROVIDES A QUALITATIVE REPRESENTATION OF THE COMMONLY OBSERVED STABILITY INCREASE AT LOW SPEEDS.

The improved stability behavior at low speeds has been attributed to an energy dissipation mechanism commonly called process damping. Process damping plays a key role in stability determination in machining processes [5–7]. Tobias and Fishwick [1], Tlusty [8] and Minis et al. [9] tried to account for process damping by including the displacement variable and its derivative in the cutting force model. Other models recognized process damping as the result of the interference between the cutting tool flank face and the undulated machined surface [5] where the amplitude of the force was assumed to be proportional to the material volume displaced due to interference [10–14]. Chiou and Liang [15] and later Clancy and Shin [16] used this model to account for process damping to capture the effect of tool wear on stability in turning. The same model was implemented by Chandiramani and Pothala [17] in their study of regenerative chatter in a two degree of freedom model for turning.

An alternative explanation for the increased stability at lower speeds was recently introduced by Stepan [18, 19]. Instead of modeling the cutting forces as a single point force, a continuous or distributed time delay model was introduced to capture the force distribution over the tool-chip interface (see Fig. 3). This paper investigates the influence of the distributed force model on the stability behavior of continuous turning. In particular, we describe an approach to transform the distributed-delay equations into a discrete-delay system. Theoretical stability investigations are performed using a state-space TFEA (temporal finite element analysis) technique [20]. Finally, different continuous-to-discrete delay ratios are used to elucidate parameter regimes where the phenomenological increased stability behavior is adequately captured.

EXAMPLE CONTINUOUS DELAY SYSTEM

In this section, a first-order scalar delay differential equation, or DDE, with both a discrete and a continuous delay is presented. Using this introductory example, the procedure of transforming the equation into a form that contains only the discrete delay is described. The stability of the resulting equation is then investigated using state-space TFEA.
Consider the first order DDE

$$\dot{x}(t)+\alpha x(t)+\beta\int_0^{t_s} x(t-\tau-\hat{t})w(\hat{t})d\hat{t}=0, \tag{1}$$

where t is time, x is a real variable, α and β are real scalars, τ is a discrete delay, $\hat{t}$ is a continuous or short delay, t_s is the duration of the short delay, and $w(\hat{t})$ is a shape or weight function. The integral in Eq. (1), as well as the existence of two types of delays, complicates the stability analysis of Eq. (1) in its current form. However, with a suitable choice of the weight function $w(\hat{t})$, Eq. (1) can be tranformed into a solvable form. In fact, a reasonble choice for $w(\hat{t})$ is

$$w(\hat{t})=e^{\frac{-\hat{t}}{\gamma\tau}}, \tag{2}$$

where $\gamma=t_s/\tau$ is the ratio of the short delay to the long one and it will be assumed to be constant. This choice of an exponential term for the weight function implies that the effect of the continuous delay disappears gradually as $t_s\to\infty$. With this choice for $w(\hat{t})$, the continuous delay term in Eq. (1) can be eliminated by first differentiating the equation with respect to time to obtain

$$\ddot{x}(t)+\alpha\dot{x}(t)+\beta\int_0^{\infty}\dot{x}(t-\tau-\hat{t})e^{\frac{-\hat{t}}{\gamma\tau}}d\hat{t}=0. \tag{3}$$

Next, integrating the continous delay term by parts gives

$$\begin{aligned}\beta\int_0^{\infty}\dot{x}(t-\tau-\hat{t})e^{\frac{-\hat{t}}{\gamma\tau}}d\hat{t} &= -\beta\Big[\,x(t-\tau-\hat{t})e^{\frac{-\hat{t}}{\gamma\tau}}\Big|_0^{\infty}\\ &\quad+\frac{1}{\gamma\tau}\int_0^{\infty}x(t-\tau-\hat{t})e^{\frac{-\hat{t}}{\gamma\tau}}d\hat{t}\,\Big]\\ &= \beta x(t-\tau)+\frac{1}{\gamma\tau}\left[\dot{x}(t)+\alpha x(t)\right].\end{aligned} \tag{4}$$

Finally, substituting Eq. (4) into Eq. (3) gives

$$\ddot{x}(t)+(\alpha+\frac{1}{\gamma\tau})\dot{x}(t)+\frac{\alpha}{\gamma\tau}\beta x(t-\tau)=0, \tag{5}$$

or in state-space form

$$\begin{bmatrix} \dot{y_1} \\ \dot{y_2} \end{bmatrix} = \begin{bmatrix} 0 & 1 \\ \frac{-\alpha}{\gamma\tau} & -\left(\alpha+\frac{1}{\gamma\tau}\right) \end{bmatrix} \begin{bmatrix} y_1 \\ y_2 \end{bmatrix} + \begin{bmatrix} 0 & 0 \\ -\beta & 0 \end{bmatrix} \begin{bmatrix} y_1(t-\tau) \\ y_2(t-\tau) \end{bmatrix}, \tag{6}$$

where now Eq. (5) represents a transformation of Eq. (1) that contains the discrete delay only. In the next section, state-space TFEA is used to investigate the stability of Eq. (5).

Stability Analysis

The stability analysis of Eq. (5) can be performed using state-space TFEA approach introduced by Mann and Patel [20]. In this approach, the expressions for the current state and the delayed state variables are written as vectors

$$\mathbf{x}_j(t) = \sum_{i=1}^{3} \mathbf{a}_{ji}^{n} \phi_i(\sigma),\ \mathbf{x}_j(t-\tau) = \sum_{i=1}^{3} \mathbf{a}_{ji}^{n-1} \phi_i(\sigma) \tag{7}$$

during the j^{th} element. These vectors represent an approximate solution for Eq. (5) in the form of a linear combination of trial functions, $\phi_i(\sigma)$. The local time, σ, varies from zero to the time of each element $t_j = \tau/E$, where E represents the number of elements used in the analysis. The chosen trial functions are orthogonalized on the interval $0 \le \sigma \le t_j$ and the use of the local time notation ensures that they remain orthogonal for every temporal element. The set of polynomial trial functions used for this analysis are

$$\phi_1(\sigma) = 1 - 23(\frac{\sigma}{t_j})^2 + 66(\frac{\sigma}{t_j})^3 - 68(\frac{\sigma}{t_j})^4 + 24(\frac{\sigma}{t_j})^5, \tag{8a}$$

$$\phi_2(\sigma) = 16(\frac{\sigma}{t_j})^2 - 32(\frac{\sigma}{t_j})^3 + 16(\frac{\sigma}{t_j})^4, \tag{8b}$$

$$\phi_3(\sigma) = 7(\frac{\sigma}{t_j})^2 - 34(\frac{\sigma}{t_j})^3 + 52(\frac{\sigma}{t_j})^4 - 24(\frac{\sigma}{t_j})^5. \tag{8c}$$

The above trial functions are obtained through interpolation, and they are constructed such that the coefficients of the assumed solution directly represent the state variable at the beginning, middle and end of each temporal element, i.e. at $\sigma = 0$, $t_j/2$ and t_j, respectively. The construction and properties of these functions are discussed in more details in [20]. For demonstration purposes, it is assumed that two elements are sufficient, i.e. $E = 2$, then the corresponding form of the assumed solution is substituted into Eq. (5) and using the method of weighted residuals a global matrix can be obtained that relates the states of the system in the current period to those in the previous period

$$\begin{bmatrix} \mathbf{I} & 0 & 0 & 0 & 0 \\ \mathbf{N}_{11}^1 & \mathbf{N}_{12}^1 & \mathbf{N}_{13}^1 & 0 & 0 \\ \mathbf{N}_{21}^1 & \mathbf{N}_{22}^1 & \mathbf{N}_{23}^1 & 0 & 0 \\ 0 & 0 & \mathbf{N}_{11}^2 & \mathbf{N}_{12}^2 & \mathbf{N}_{13}^2 \\ 0 & 0 & \mathbf{N}_{21}^2 & \mathbf{N}_{22}^2 & \mathbf{N}_{23}^2 \end{bmatrix} \begin{bmatrix} a_{11} \\ a_{12} \\ a_{21} \\ a_{22} \\ a_{23} \end{bmatrix}^n = \begin{bmatrix} 0 & 0 & 0 & 0 & \mathbf{I} \\ \mathbf{P}_{11}^1 & \mathbf{P}_{12}^1 & \mathbf{P}_{13}^1 & 0 & 0 \\ \mathbf{P}_{21}^1 & \mathbf{P}_{22}^1 & \mathbf{P}_{23}^1 & 0 & 0 \\ 0 & 0 & \mathbf{P}_{11}^2 & \mathbf{P}_{12}^2 & \mathbf{P}_{13}^2 \\ 0 & 0 & \mathbf{P}_{21}^2 & \mathbf{P}_{22}^2 & \mathbf{P}_{23}^2 \end{bmatrix} \begin{bmatrix} a_{11} \\ a_{12} \\ a_{21} \\ a_{22} \\ a_{23} \end{bmatrix}^{n-1}, \tag{9}$$

which can be written in a more compact form as

$$\mathbf{H}\,\mathbf{a}_n = \mathbf{G}\,\mathbf{a}_{n-1} \tag{10}$$

where $\mathbf{I}$ is a 2×2 identity matrix. The terms $\mathbf{N}_{pi}^j$ and $\mathbf{P}_{pi}^j$ are the following square matrices

$$\mathbf{N}_{pi}^j = \int_0^{t_j} \left(\mathbf{I}\dot{\phi}_i(\sigma) - \mathbf{C}\phi_i(\sigma)\right)\psi_p(\sigma)d\sigma, \tag{11a}$$

$$\mathbf{P}_{pi}^j = \int_0^{t_j} \left(\mathbf{D}\phi_i(\sigma)\right)\psi_p(\sigma)d\sigma, \tag{11b}$$

The functions $\psi_p(\sigma)$ are called test functions, or weighting functions. These functions are used to minimize the error incurred from the solution approximation. The weighting functions used for the presented analysis were shifted Legendre polynomials. These polynomials were used because they satisfy the required condition of linear independence. Here, only the first two shifted Legendre polynomials, $\psi_1(\sigma) = 1$ and $\psi_2(\sigma) = 2(\sigma/t_j) - 1$, will be used to keep the resulting matrices square.

Recalling that the coefficients of the assumed solution directly represent the state variable at various points in time, Eq. (10) can alternatively be written as $\mathbf{x}_n = \mathbf{Q}\mathbf{x}_{n-1}$, where $\mathbf{Q} = \mathbf{H}^{-1}\mathbf{G}$ is called the monodromy operator. This expression represents a discrete solution form for Eq. (1) that maps the states of the system over a single delay period, from the $n-1$ period to the n^{th} period. Here, the condition for asymptotical stability requires that all the characteristic multipliers, or eigenvalues of $\mathbf{Q}$, must lie within the unit circle of the complex plane. For more details about this technique and for convergence properties the reader is referred to reference [20]. Figure (2) shows the stability chart for Eq. (1) for $\gamma = 0.5$ and 1.5 assuming a discrete delay $\tau = 1$.

In the next section the same analysis will be carried out for a continuous turning model.

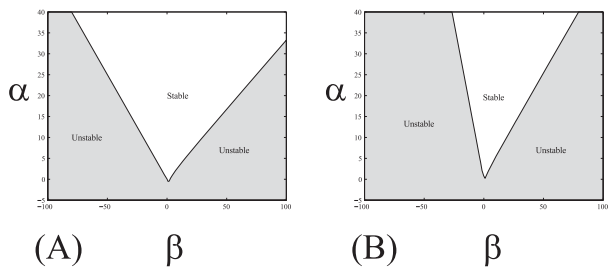

Figure 2. STABILITY CHARTS OF Eq. (1) FOR $\tau = 1$, AND (A) $\gamma = 0.5$ AND (B) $\gamma = 1.5$. MOREOVER, A GRID OF 100×100 AND E=10 WERE USED. UNSTABLE REGIONS ARE SHADED WHILE STABLE REGIONS ARE LEFT UNSHADED.

CONTINUOUS TURNING MODEL

The governing equation of motion for a rigid workpiece and a tool compliant in one direction, $z(t)$, is

$$m\ddot{z} + c\dot{z} + kz = -F_z(A), \tag{12}$$

where m, c and k are the modal mass, stiffness and damping respectively, and $F_z(A)$ is the cutting force component along the z direction as a function of the instantaneous chip area, $A(t)$. The instantaneous chip area is the product of the depth of cut, b, and the instantaneous chip thickness, $h(t)$, i.e. $A(t) = bh(t)$.

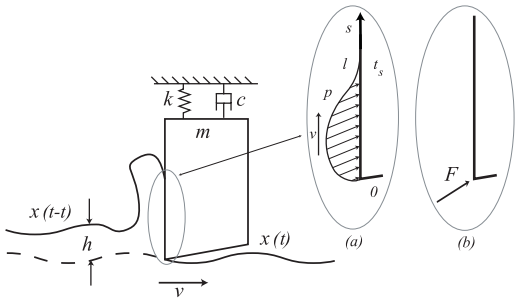

Figure 3. SCHEMATIC DIAGRAM OF A: (A) DISTRIBUTED FORCE MODEL AND (B) CONVENTIONAL POINT FORCE MODEL. CASE (A) USES A STRESS DISTRIBUTION OVER THE TOOL RAKE FACE AND APPLIES A FINITE TIME FOR THE CHIP TO TRAVEL ALONG THE TOOL-CHIP INTERFACE. CASE (B) IS THE CONVENTIONAL MODELING APPROACH OF USING A POINT FORCE AND A DISCRETE DELAY MODEL.

Let z^* be the zero solution for the system, which corresponds to cutting at the nominal depth of cut h_o. Under these conditions, the system is in equilibrium with the static cutting force, f_o. Then for any other solution, $z(t)$, one can write [21]

$$z(t) = z^* + \xi(t), \tag{13}$$

where $\xi(t)$ represents a perturbation of the equilibrium solution. The growth or decay of such small perturbations determines the stability of the original system, Eq. (12). Similarly, the cutting force can be described as the summation of a static component and a dynamic variation due to oscillations

$$F_z(A) \approx f_o + \Delta F_z(A) \tag{14a}$$
$$\approx -kz^* + \Delta F_z(A), \tag{14b}$$

Equations (13) and (14) are substituted into Eq. (12) to obtain the variational equation

$$m\ddot{\xi}(t) + c\dot{\xi}(t) + k\xi(t) \approx -\Delta F_z(A). \tag{15}$$

Dropping the approximation sign and dividing by the mass, m, Eq. (15) becomes

$$\ddot{\xi}(t) + 2\zeta\omega_n\dot{\xi}(t) + \omega_n^2\xi(t) = -\frac{1}{m}\Delta F_z(A), \tag{16}$$

where $\omega_n = \sqrt{k/m}$ is the angular natural frequency, $\zeta = c/(2m\omega_n)$ is the damping ratio, and $\Delta F_z(A)$ is the dynamic force variation. The expression for the force variation depends on the adopted force model, i.e. conventional point force model or distributed force model. In the next section, the conventional point force model will be used in conjunction with Eq. (16) to produce an equation that can be solved for stability regions.

Point Force Model

In the conventional point force model, cutting forces are characterized by a single force vector acting at a single point–the tool tip. This force is assumed to be a function of the instantaneous chip area, $A(t)$, (see Fig. 4).

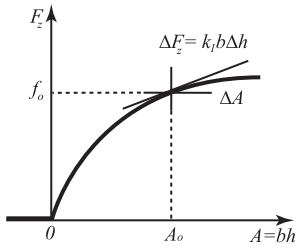

Figure 4. CUTTING FORCE AND CHIP AREA RELATION.

The dynamic force variation is written as a Taylor series expansion around the nominal uncut chip area A_o

$$\Delta F_z(A) = u(t)\ (F_z(A) - f_o) = \sum_{j=1}^{p} k_j (\Delta A)^j \tag{17}$$

where for continuous turning the tool is assumed to be in the cut all the time and a force proportional to the uncut chip area acts on the tool. The chip area variation is

$$\Delta A = A - A_o = b(h - h_o). \tag{18}$$

The coefficients of the power series in Eq. (17) come from

$$k_j = \frac{1}{j!} \frac{d^j F_z(A_o)}{dA^j},\ j = 1, 2, \ldots \tag{19}$$

The first coefficient, k_1, in the above expression is referred to as the cutting coefficient and is usually determined experimentally. k_1 represents the linear approximation of the cutting force variation, while the higher order terms, k_2–k_∞, provide higher order approximations.
The linear approximation of the cutting force variation is inserted into Eq. (16) to obtain

$$\ddot{\xi}(t) + 2\zeta\omega_n \dot{\xi}(t) + \omega_n^2 \xi(t) = -\frac{k_1 b}{m}(h(t) - h_o). \tag{20}$$

Substituting $h(t) = h_o + \xi(t) - \xi(t-\tau)$ into Eq. (20) gives

$$\ddot{\xi}(t) + 2\zeta\omega_n \dot{\xi}(t) + \omega_n^2 \xi(t) = -\frac{k_1 b}{m}(\xi(t) - \xi(t-\tau)) \tag{21}$$

which represents a DDE with constant coefficients. A set of dimensionless parameters for time, spindle speed, time delay and depth of cut is defined as [22]

$$\tilde{t} = \omega_n t,\ \ \tilde{\Omega} = \frac{\Omega}{\omega_n},\ \ \tilde{\tau} = \omega_n \tau,\ \ \tilde{b} = \frac{b k_1}{m\omega_n^2}. \tag{22}$$

These substitutions result in the dimensionless characteristic frequency $\tilde{\omega}_n = 1$. The non-dimensionalized version of Eq. (21) then reads

$$\ddot{\xi}(\tilde{t}) + 2\zeta\dot{\xi}(\tilde{t}) + \xi(\tilde{t}) = -\tilde{b}(\xi(\tilde{t}) - \xi(\tilde{t} - \tilde{\tau})). \tag{23}$$

Figure 5 shows two stability charts that were obtained using state-space TFEA with Eq. (23) for the point force model. Two cases were considered: one of a relatively high damping ratio, $\zeta = 0.02$, and another for a relatively low damping ratio, $\zeta = 0.0038$. The region below the boundary line represents stable cutting conditions, while that above the boundary line corresponds to unstable cutting process. It can be seen that at low speeds, this model does not capture the improved stability encountered in practice. Please note that for all turning stability plots, a square grid of 600×600 points was used.

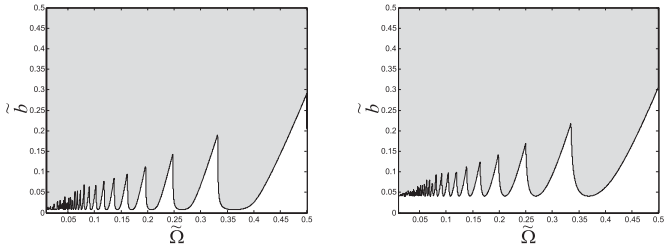

(a) $\zeta = 0.0038$ (b) $\zeta = 0.02$

Figure 5. STABILITY CHARTS FOR THE POINT FORCE MODEL OF CONTINUOUS TURNING PLOTTED AS A FUNCTION OF THE NON-DIMENSIONALIZED CUTTING SPEED AND DEPTH OF CUT. THE DAMPING RATIOS USED ARE (A) $\zeta = 0.0038$ AND (B) $\zeta = 0.02$, (UNSTABLE REGIONS SHADED).

Distributed Force Model

The distributed force model reflects a more realistic representation of the physical cutting forces in turning. Instead of concentrating the cutting forces at a single point, these forces are assumed to have a distribution per unit length, P_z, with varying magnitudes along the tool-chip interface. The cutting forces can be described in terms of this distribution by

$$F_z(A) = \int_0^l P_z(A, s) ds, \tag{24}$$

where s is a local coordinate whose origin is fixed to the tool tip. This local coordinate describes the contact distance between the sliding chip and the active face of the tool. The range of values for s is from 0 to the length which represents the location where the chip separates from the tool, l. One approximation for P_z combines the Taylor approximation of the cutting force with an estimated shape function W (with unit $1/m$)

$$P_z(A, s) = F_z(A) W(s),\ \ s \in [0, l]. \tag{25}$$

In order to ensure that this new model maintains the mechanics of the system; substituting $A = A_o$, which corresponds to cutting

under stationary conditions, should yield a value of $f_o = F_z(A_o)$. Imposing this constraint on equation (24) gives

$$F_z(A_o) = \int_0^l P_z(A_o, s)ds = F_z(A_o)\int_0^l W(s)ds,$$

$$\Rightarrow \int_0^l W(s)ds = 1. \tag{26}$$

Equation (26) provides a fundamental condition which has to be satisfied by any chosen shape function. Let τ be the discrete time delay associated with the tool passage period, and let a short continuous time delay t_s be introduced such that

$$\tau = \frac{d_o\pi}{v} = \frac{2\pi}{\Omega},\ t_s = \frac{l}{v_c} = \frac{l}{r_c v}, \tag{27}$$

where $d_o\pi$ is the circumference of the cylindrical workpiece, Ω is the angular velocity of the workpiece in units of rad/s, r_c is the chip thickness ratio and $v_c = r_c v$ is the chip speed over the rake face [23]. It follows that the ratio of the short time delay t_s to the long one τ is constant

$$r = \frac{t_s}{\tau} = \frac{l}{r_c d_o \pi}.$$

The shape of the stress distribution can be expressed in the time domain by introducing a local time $\hat{t} = s/v_c$. Substituting $\hat{t}$ into Eq. (26) yields the following condition on the shape function in the local time domain

$$\int_0^{t_s} w(\hat{t})d\hat{t} = 1. \tag{28}$$

This local time, $\hat{t} \in [0, t_s]$, gives how much earlier in time a certain segment of the chip flowing over the active tool face was being cut at the tip of the tool as shown in Fig. 6. The assumption that the chip flows at a speed, $v_c = r_c v$, means that the area of a section of the chip above the tool tip at a local time $\hat{t}$ is equal to the area of the same chip section as it was being cut at the tool tip at $t - \hat{t}$ time units ago, or

$$A(t,\hat{t}) = b(h_o + \xi(t-\hat{t}) - \xi(t-\tau-\hat{t})),\ t \in [t_o, \infty),\ \hat{t} \in [0, t_s], \tag{29}$$

where $A(t,\hat{t})$ defines the chip area at time t and local time $\hat{t}$. At $\hat{t} = 0$, Eq. (29) gives back the regular expression for the chip area at the tool tip

$$A(t,0) = b(h_o + \xi(t) - \xi(t-\tau)).$$

The cutting force distribution can now be expressed in the z direction in the time domain using the global time t and the local one $\hat{t}$

$$p_z(t,\hat{t}) = P_z(A(t,\hat{t}), v_c\hat{t}) = F_z(A(t,\hat{t}))\frac{1}{v_c}w(\hat{t}),\ t \in [t_o, \infty),\ \hat{t} \in [0, t_s]. \tag{30}$$

Substituting the above results; Eqs. (24), (28), (30), the power

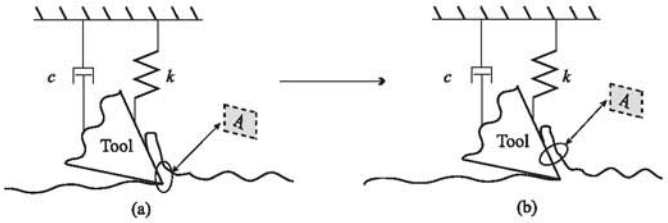

Figure 6. SHORT TIME DELAY EMBEDDING INTO THE FORCE MODEL. THE AREA OF A CERTAIN SEGMENT OF THE CHIP FLOWING OVER THE RAKE FACE IN (B) CAN BE DESCRIBED BY THE AREA OF THE SAME SEGMENT AS IT WAS BEING CUT AT THE TOOL TIP IN (A) AT TIME $t - \hat{t}$.

series from Eq. (17) and also the chip area from Eq. (29), the cutting force variation in the z direction reads

$$\Delta F_z(A(t,\hat{t})) \approx \int_0^{t_s}\sum_{j=1}^{p} k_j b^j (\xi(t-\hat{t}) - \xi(t-\tau-\hat{t}))^j w(\hat{t})d\hat{t} \tag{31}$$

$$\approx k_1 b \int_0^{t_s} (\xi(t-\hat{t}) - \xi(t-\tau-\hat{t}))\, w(\hat{t})d\hat{t}, \tag{32}$$

where equation (32) is the expression for the linearized cutting force variation. Substitution of equation (32) into the variational equation of motion (16) gives

$$\ddot{\xi} + 2\zeta\omega_n\dot{\xi} + \omega_n^2\xi = -\frac{k_1 b}{m}\int_0^{t_s} (\xi(t-\hat{t}) - \xi(t-\tau-\hat{t}))w(\hat{t})\, d\hat{t}. \tag{33}$$

The integro-differential form of Eq. (33) is now similar to that of Eq. (1); hence, by choosing an exponential weight function for the distributed cutting force system and following the steps outlined previously, an order increment and a stability analysis of the system can be performed. Assume that this exponential shape function, $w(\hat{t})$, is of the form

$$w(\hat{t}) = \frac{v_c}{l}\exp(\frac{-v_c}{l}\hat{t}) = \frac{1}{r\tau}\exp(\frac{-\hat{t}}{r\tau}),\ \hat{t} \in [0, \infty). \tag{34}$$

Consequently, the third order tranformation of Eq. (33) which contains only the discrete delay reads

$$\overset{(3)}{\xi}(\tilde{t}) + (\frac{1}{r\tilde{\tau}} + 2\zeta)\ddot{\xi}(\tilde{t}) + (\frac{2\zeta}{r\tilde{\tau}} + 1)\dot{\xi}(\tilde{t}) + \frac{1}{r\tilde{\tau}}(1+\tilde{b})\xi(\tilde{t}) - \frac{\tilde{b}}{r\tilde{\tau}}\xi(\tilde{t}-\tilde{\tau}) = 0, \quad (35)$$

where the parameters defined in Eq. (22) were used to obtain the above non-dimensional equation. Figure 7 shows two stability plots that were obtained using state-space TFEA with Eq. (35) for the distributed force model. These plots were generated for a very-low value of the delay ratio, $r = 0.001$, and they can be compared directly to their point force model counterparts in Fig. 5. It can be seen that the distributed force model gives results similar to the point force model when the delay ratio is very small, i.e when the short delay is negligible compared to the discrete delay. However, for larger values of r, Figure 8 shows an improved stability behavior at lower speeds.

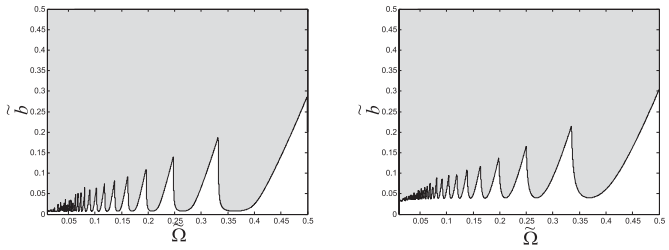

(a) $\zeta = 0.0038$ (b) $\zeta = 0.02$

Figure 7. STABILITY CHARTS FOR THE DISTRIBUTED FORCE MODEL OF CONTINUOUS TURNING PLOTTED AS A FUNCTION OF THE NON-DIMENSIONALIZED CUTTING SPEED AND DEPTH OF CUT. THE DELAY RATIO USED is $r = 0.001$, AND THE DAMPING RATIOS USED ARE (A) $\zeta = 0.0038$ AND (B) $\zeta = 0.02$, (UNSTABLE REGIONS SHADED).

DISCUSSION

This paper investigates the analysis of delay integro-differential equations to explain the increased stability behavior commonly observed at low cutting speeds. In literature, this improved stability has been attributed to the interference between the workpiece and the tool relief face. In past work, the energy dissipation through such an interference mechanism has been called process damping. The present manuscript has described and investigated an alternative physical explanation. A distributed cutting force model, along with an exponential distribution over the tool-chip interface, is assumed. Although a distributed force model is more realistic, this idea contrasts the standard approach of using a point force. In addition, the distributed

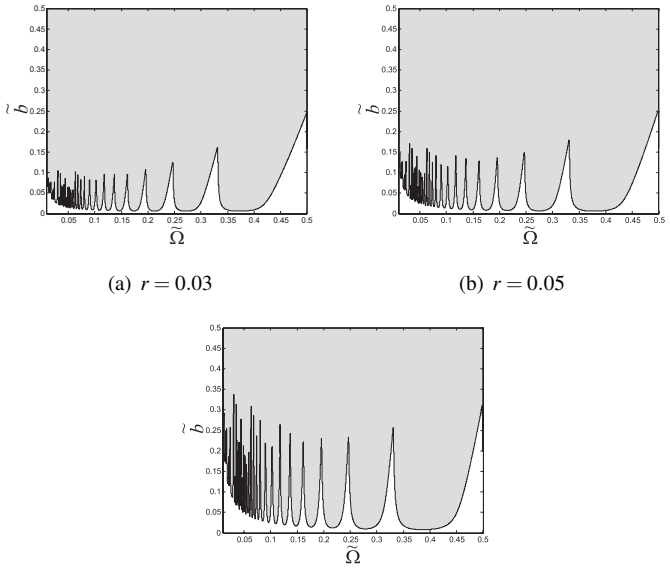

(a) $r = 0.03$ (b) $r = 0.05$

(c) $r = 0.10$

Figure 8. STABILITY CHARTS FOR THE DISTRIBUTED FORCE MODEL OF CONTINUOUS TURNING PLOTTED AS A FUNCTION OF THE NON-DIMENSIONALIZED CUTTING SPEED AND DEPTH OF CUT. THE DAMPING RATIO USED IS $\zeta = 0.0038$, AND THE DELAY RATIOS USED ARE (a) $r = 0.03$, (B) $r = 0.05$ AND (C) $r = 0.10$, (UNSTABLE REGIONS SHADED).

force model results in a more complicated governing equation, a second order delayed integro-differential equation, that involves both a discrete and continuous delay. The continuous delay results from the finite time it takes the chip to slide along the rake face of the tool while the discrete delay is from the period between consecutive passages of the cutting tooth.

The continuous delay has been an un-modeled parameter that was shown to have a great impact on low-speed cutting stability. An exponential shape function was proposed to approximate the force distribution over the tool-chip contact length, and a constant delay ratio was introduced to describe the ratio between the continuous and the discrete delays. An approach was described to transform the governing equation of motion into a third order discrete system. The state-space representation of the new system was then obtained, and the state-space TFEA technique was used to chart the stability boundaries for continuous and interrupted turning. Different delay ratios were used for generating stability charts to study the effect of the continuous delay on stability. For comparison purposes, the point force model was used to obtain the conventional stability charts for continuous turning.

It was found that for a small value of the delay ratio, i.e. when the continuous delay is negligible in comparison to the discrete one, the predicted stability boundaries were similar to those of the point force model. However, for larger values of the delay ratio, the distributed force model showed an improved sta-

bility behavior at lower speeds when compared to the point force model. The stable parameter space continued to increase with increases in the delay ratio which confirms the stabilizing effect of the continuous delay.

Possible tasks for future research include experimental verification of the results presented in this study. Moreover, the additional damping attributed to the interaction between the tool nose and the undulated machined surface can also be approximated using the presented approach. Current literature estimates these forces through the calculation of the volume displaced due to the interaction. However, another option would be to assume that there is a force distribution of some shape on the clearance face as well. The presented results can then be used to include the effect of these forces in the system model. Another future task is to construct a solution strategy that can accommodate different shape functions for the force distribution, and to expand these solution techniques to other application areas.

ACKNOWLEDGMENT

Support from U.S. National Science Foundation CAREER Award (CMS-0636641) and the Janos Bolyai Research Scholarship of the Hungarian Academy of Sciences is gratefully acknowledged.

REFERENCES

[1] Tobias, S. A., and Fishwick, W., 1958. "Theory of regenerative machine tool chatter". *Engineering,* **205**.

[2] Cook, N. H., 1959. "Self-excited vibrations in metal cutting". *Journal of Engineering for Industry,* **81**, pp. 183–186.

[3] Tlusty, J., and Polacek, M., 1963. "The stability of machine tools against self-excited vibrations in machining". In Proceedings of the ASME International Research in Production Engineering, pp. 465–474.

[4] Merrit, H. E., 1965. "Theory of self-excited machine-tool chatter, contribution to machine-tool chatter research - 1". *Journal of Engineering for Industry,* **87**, pp. 447–454.

[5] Sisson, T. R., and Kegg, R. L., 1969. "An explanation of low-speed chatter effects". *Journal of Engineering for Industry,* **91**(4), pp. 951–958.

[6] Tlusty, J., and Heczko, O., 1980. "Improving tests of damping in the cutting process". In Proceedings of the 8th North American Manufacturing Research Conference, SME, pp. 372–376.

[7] Balakrishnan, P., k. F. Eman, and Wu, S. M., 1981. "Analysis of cutting process damping". In Proceedings of the 9th North American Manufacturing Research Conference, SME, p. 247.

[8] Tlusty, J., 1978. "Analysis of the state of research in cutting dynamics". *Annals of CIRP,* **27**(2), pp. 583–589.

[9] Minis, I., Magrab, E., and Pandelidis, I., 1990. "Improved methods for the prediction of chatter in turning, part 2: determination of cutting process parameters". *Journal of Engineering for Industry,* **112**(1), pp. 21–27.

[10] Wu, D. W., 1988. "Application of a comprehensive dynamic cutting force model to orthogonal wave-generating processes". *International Journal of Mechanical Sciences,* **30**(8), pp. 581–600.

[11] Jemielniak, K., and Widota, A., 1989. "Numerical simulation of non-linear chatter vibration in turning". *International Journal of Machine Tools and Manfacture,* **29**(2), pp. 239–247.

[12] Shaw, M., and DeSalvo, G. J., 1970. "On the plastic flow beneath a blunt axisymmetric indenter". *Journal of Engineering for Industry,* **92**, pp. 480–494.

[13] Tarng, Y. S., Young, H. T., and Lee, B. Y., 1994. "An analytical model of chatter vibration in metal cutting". *International Journal of Machine Tools and Manfacture,* **34**(2), pp. 183–197.

[14] Lee, B. Y., Tarng, Y. S., and Ma, S. C., 1995. "Modeling of the process damping force in chatter vibration". *International Journal of Machine Tools and Manfacture,* **35**(7), pp. 951–962.

[15] Chiou, R. Y., and Liang, S. Y., 1998. "Chatter stability of a slender cutting tool in turning with tool wear effects". *International Journal of Machine Tools and Manfacture,* **38**(4), pp. 315–327.

[16] Clancy, B. E., and Shin, Y. C., 2002. "A comprehensive chatter prediction model for face turning operation including tool wear effect". *International Journal of Machine Tools and Manfacture,* **42**(9), pp. 1035–1044.

[17] Chandiramani, N. K., and Pothala, T., 2006. "Dynamics of 2-dof regenerative chatter during turning". *Journal of Sound and Vibration,* **290**, pp. 448–464.

[18] Stépán, G., 1989. *Retarded Dynamical Sytems: Stability and Characteristic Functions*. John Wiley & Sons.

[19] Stépán, G., 1997. *Dynamics and Chaos in Manufacturing Processes*, 1 ed. Wiley, New York, ch. Delay-differential equation models for machine tool chatter., pp. 165–192.

[20] Mann, B., and Patel, B., 2008. "Stability of delay equations written as state space models". *Journal of vibration and control*. Accepted.

[21] Jordan, D. W., and Smith, P., 1999. *Nonlinear ordinary differential equations: an introduction to dynamical systems*, third ed. Oxford University Press, Oxford.

[22] Szalai, R., and Stépán, G., 2006. "Lobes and lenses in the stability chart of interrupted turning". *Journal of Computational and Nonlinear Dynamics,* **1**, pp. 205–211.

[23] Altintas, Y., 2000. *Manufacturing Automation*, 1 ed. Cambridge University Press, New York.